

An Eulerian finite element formulation for modeling stationary finite strain elastic deformation processes

Dolores Demarco and Eduardo N. Dvorkin
Center for Industrial Research, FUDETEC
Av. Córdoba 320
1054 Buenos Aires, Argentina

Abstract

A new finite element formulation, aimed at the modeling of stationary finite strain elastic deformation processes is presented. The new formulation is based on an Eulerian description of motion and on the transport of the deformation gradient tensor.

1 Introduction

Most of the new technological developments in metal forming rely on the computational modeling of the deformation processes in order to analyze the effect of different set-up options, of different forming tools, of different lubrication conditions, etc. In Ref. [1] some experiences related to the steel industry are discussed.

For modeling bulk metal forming processes, in those cases where the elastic strains can be neglected, the *flow formulation* [2] (rigid-viscoplastic material models [3]) is normally used.

At our research center we have implemented, for analyzing transient and stationary metal forming processes, the flow formulation using an Eulerian description of motion with a fixed mesh and the material moving inside that mesh [4] [5] via the pseudo-concentrations technique [6] [7]. The main advantages of this implementation are that it is very efficient and that it does not require remeshing techniques. Regarding its use in technological analyses, the developed finite element formulation was implemented in our code METFOR and it is being used for analyzing the hot rolling of steel products ([8] to [11]) and the continuous casting of steel slabs [12].

However, in the analysis of some bulk metal forming processes it is not possible to neglect the elastic deformations, e.g. the cold rolling of steel plates, either because the elastic spring-back plays an important role in the process or because the residual stresses need to be determined. Hence, it is desirable to develop an Eulerian formulation for modeling stationary deformation processes, with the capability of incorporating elastic effects.

Some attempts for a-posteriori estimations of the elastic effects, on the basis of the results provided by the flow formulation, have been presented in the literature [13]; also some attempts for including the elastic effects using a hypoelastic formulation to model the elastic behavior have been published [14].

In this paper we discuss a finite element formulation, suitable for modeling stationary elastic finite deformation processes, that is based on an Eulerian description of motion and on a hyperelastic constitutive relation. In a different numerical environment, a similar Continuum Mechanics formulation has been presented in [15].

In the second section of the paper we present the Continuum Mechanics formulation and in the third one its finite element implementation. The developed numerical algorithm is discussed in the fourth section and demonstrative numerical examples are presented in the fifth one.

It is worth highlighting that the formulation that we develop in this paper is the basis for the ongoing development of an elasto-plastic finite strain Eulerian formulation via the pseudo-concentrations technique.

2 The Continuum Mechanics formulation

2.1 The Eulerian description of motion

In the spatial configuration corresponding to time t [16] we use a Cartesian coordinate system $\{^t x_j, j = 1, 2, 3\}$ and at a given point a particle material velocity is given by,

$${}^t \mathbf{v} = {}^t \mathbf{v}({}^t x_j, t). \quad (1)$$

In the t -configuration the following partial differential equations need to be satisfied,

- **Momentum balance equations:**

In an Eulerian framework, the equilibrium equations are [16],

$${}^t \rho \left(\frac{\partial {}^t \mathbf{v}}{\partial t} + {}^t \mathbf{v} \cdot \nabla {}^t \mathbf{v} \right) = {}^t \rho {}^t \mathbf{f}^V + \nabla \cdot {}^t \underline{\underline{\boldsymbol{\sigma}}}. \quad (2)$$

In the above $\nabla = \left(\frac{\partial}{\partial {}^t x_k} {}^t \mathbf{e}_k \right)$, where the ${}^t \mathbf{e}_k$ are the ortho-normal base vectors of the Cartesian system, also

${}^t \rho$: density.

${}^t \underline{\underline{\boldsymbol{\sigma}}}$: Cauchy stress tensor.

${}^t \mathbf{f}^V$: external volumetric load vector.

- **Continuity equation:**

$$\frac{\partial {}^t J}{\partial t} + {}^t \mathbf{v} \cdot \nabla {}^t J - {}^t J \nabla \cdot {}^t \mathbf{v} = 0. \quad (3)$$

Where, ${}^t J = \frac{{}^o \rho}{{}^t \rho}$ and ${}^o \rho$ is the density of the reference configuration ($t = 0$). Using Cartesian coordinates it is immediate to show that [16] [17],

$${}^t J = \det [{}^t \underline{\underline{\mathbf{E}}}], \quad (4)$$

where ${}^t \underline{\underline{\mathbf{E}}}$ is the deformation gradient tensor.

- **Deformation gradient transport:**

The material time derivative of the deformation gradient tensor is [16],

$$\frac{D {}^t \underline{\underline{\mathbf{E}}}}{D t} = \frac{\partial {}^t \underline{\underline{\mathbf{E}}}}{\partial t} + {}^t \mathbf{v} \cdot \nabla {}^t \underline{\underline{\mathbf{E}}} = {}^t \underline{\underline{\mathbf{l}}} \cdot {}^t \underline{\underline{\mathbf{E}}}. \quad (5)$$

In the above equation we introduce the velocity gradient tensor, ${}^t \underline{\underline{\mathbf{l}}}^T = \nabla {}^t \mathbf{v}$.

Also for the isochoric part of the deformation gradient we have,

$${}^t \underline{\underline{\hat{\mathbf{E}}}} = {}^t J^{-\frac{1}{3}} {}^t \underline{\underline{\mathbf{E}}} \quad (6a)$$

$$\frac{\partial {}^t \underline{\underline{\hat{\mathbf{E}}}}}{\partial t} + {}^t \mathbf{v} \cdot \nabla {}^t \underline{\underline{\hat{\mathbf{E}}}} = \left[{}^t \underline{\underline{\mathbf{l}}} - \frac{1}{3} (\nabla \cdot {}^t \mathbf{v}) {}^t \underline{\underline{\mathbf{g}}} \right] \cdot {}^t \underline{\underline{\hat{\mathbf{E}}}} \quad (6b)$$

The tensor ${}^t \underline{\underline{\mathbf{g}}}$ is the metric tensor of the spatial configuration, in our case it is a Cartesian metric tensor and $\left[\det \left({}^t \underline{\underline{\hat{\mathbf{E}}}} \right) \right] = 1$.

It is important to realize that the fulfillment of Eqn.(5) implies the fulfillment of Eqns.(3 and 6b)

- **Integral form of the Continuum Mechanics equations:**

Momentum balance equations

For “slow” deformation processes we can neglect the inertia terms and considering an admissible spatial velocity field $\delta \underline{\mathbf{v}}$ [18] we can write Eqn. (2) as,

$$\int_{{}^tV} \left[{}^t\rho \, {}^t\mathbf{f}^V + \underline{\mathbf{\nabla}} \cdot {}^t\underline{\boldsymbol{\sigma}} \right] \cdot \delta \underline{\mathbf{v}} \, {}^tdv = 0. \quad (7)$$

In the above equation, tV is the volume of the spatial configuration. Using the divergence theorem we get,

$$\int_{{}^tV} \delta \underline{\mathbf{v}} \cdot {}^t\rho \, {}^t\mathbf{f}^V \, {}^tdv + \int_{{}^t\partial V} \delta \underline{\mathbf{v}} \cdot {}^t\underline{\boldsymbol{\tau}} \, {}^tdv - \int_{{}^tV} \delta \underline{\mathbf{1}} : {}^t\underline{\boldsymbol{\sigma}} \, {}^tdv = 0 \quad (8)$$

where ${}^t\partial V$ is the boundary of the spatial configuration and ${}^t\underline{\boldsymbol{\tau}} = {}^t\underline{\mathbf{n}} \cdot {}^t\underline{\boldsymbol{\sigma}}$ is the traction vector on a surface with external normal ${}^t\underline{\mathbf{n}}$.

Equation (8) is the weak form of the momentum balance equations when the inertia forces are neglected.

Transport of the deformation gradient

For the transport of the deformation gradient tensor, the weak form is obtained via a weighted residuals technique [19]. For each component of ${}^t\underline{\mathbf{F}}$ in the fixed Cartesian system we get, from Eqn. (5)

$$\int_{{}^tV} w_p^{PG} \left[\frac{\partial {}^tF_{ij}}{\partial t} + {}^tv_k \frac{\partial}{\partial {}^tx_k} {}^tF_{ij} - {}^tl_{im} \, {}^tF_{mj} \right] {}^tdv = 0. \quad (9)$$

In the above equation the w_p^{PG} are the SUPG weighting functions [19] [20] [21] and the index p goes from one to the number of nodes of the finite element discretization (*NNODES*).

2.2 The hyperelastic constitutive relation

For an isotropic elastic material with finite deformations we use the elastic energy function proposed by Simo [18] [22]:

$${}^tW = {}^tU({}^tJ) + \frac{1}{2}G \, tr \left({}^t\hat{\underline{\mathbf{b}}} \right) \quad (10a)$$

$${}^tU({}^tJ) = \frac{1}{2}K \left(\ln {}^tJ \right)^2. \quad (10b)$$

In the above equations tW is the energy density per unit volume of the reference configuration, (K, G) are material constants and,

$${}^t\hat{\underline{\mathbf{b}}} = {}^t\underline{\hat{\mathbf{E}}} \cdot {}^t\underline{\hat{\mathbf{E}}}^T \quad (11)$$

is the isochoric part of the Finger deformation tensor.

This model may be regarded as an extension to the compressible range of the neo-Hookean model.

We can write the second Piola-Kirchhoff stress tensor corresponding to the time t and referred to the reference configuration ($t = 0$) as [23],

$${}^t\underline{\mathbf{S}} = 2 \frac{\partial {}^tW}{\partial {}^t\underline{\mathbf{C}}}. \quad (12)$$

In the above equation ${}^t\underline{\mathbf{C}}$ is the Green deformation tensor.

Doing a push-forward of the Cartesian components of the second Piola-Kirchhoff stress tensor we get the Cartesian components of the Kirchhoff stress tensor (${}^t\underline{\boldsymbol{\tau}}$) [17],

$${}^t\tau_{ij} = {}^tF_{il} {}^tS_{lm} {}^tF_{jm} . \quad (13)$$

After some algebra we get for the Cauchy stress components,

$${}^t\sigma_{ij} = ({}^tJ)^{-1} \left[K \ln ({}^tJ) \delta_{ij} + G \operatorname{dev} \left({}^t\hat{b} \right)_{ij} \right] \quad (14)$$

where $\operatorname{dev}(\cdot)$ calculates the deviatoric part of the tensor between brackets.

3 The finite element formulation

In this section we are going to discretize the problem outlined in the previous section using the finite element method.

3.1 Discretization of the deformation gradient transport equations

To discretize the Eqns. (9) we use for the interpolation of the deformation gradient components:

$${}^tF_{ij}(r_l, t) = h_k(r_l) {}^tF_{ij}^k(t) \quad (15)$$

where $h_k(r_l)$ are the isoparametric 3D interpolation functions, $\{r_l, l = 1, 2, 3\}$ are the natural coordinates of a point inside the element [24] and ${}^tF_{ij}^k$ are the nodal point values. As usual the repeated index k indicates a summation over all the nodes.

From Eqn.(9) we get an algebraic system of $9 * NNODES$ equations; the solution of this equations system is straightforward using either a direct or iterative solver. An alternative approach that requires the solution of 3 uncoupled systems of $3 * NNODES$ equations each, was presented in Ref.[25].

3.2 Discretization of the momentum balance equations

We use for the interpolation of the velocity field,

$${}^t\mathbf{v}(r_l, t) = h_k(r_l) {}^t\mathbf{v}^k(t) \quad (16)$$

where the ${}^t\mathbf{v}^k$ are the nodal point velocity vectors. Replacing in Eqn. (8) we get,

$$\delta v_i^k \left[\int_{tV} h_k {}^t\rho {}^t\mathbf{f}_i^V {}^t dv + \int_{t\partial V} h_k {}^t\mathbf{t}_i {}^t dv \right] = \delta v_i^k \int_{tV} \frac{\partial h_k}{\partial {}^tx_j} {}^t\sigma_{ij} {}^t dv . \quad (17)$$

Hence, being the equivalent external nodal forces vector at time t :

$$[{}^tR^{ext}]_i^k = \int_{tV} h_k {}^t\rho {}^t\mathbf{f}_i^V {}^t dv + \int_{t\partial V} h_k {}^t\mathbf{t}_i {}^t dv \quad (18)$$

and the internal one,

$$[{}^tR^{int}]_i^k = \int_{tV} \frac{\partial h_k}{\partial {}^tx_j} {}^t\sigma_{ij} {}^t dv . \quad (19)$$

We next consistently project the deformation fields obtained from Eqns. (9, 4, 6a) for their use in the momentum balance equations.

3.2.1 Projections of tJ and $\frac{\partial {}^tJ}{\partial t}$

From the solution of Eqns.(9) we determine the value of $\det({}^t\mathbf{E})$ at each element node and, from these values,

$${}^tJ(r_i, t) = h_k(r_i) \left(\det({}^t\mathbf{E})^k \right) (t) . \quad (20)$$

Let us consider ${}^t\Theta(r_i, t)$ to be a projection of ${}^tJ(r_i, t)$. Using a new set of interpolation functions $\widehat{h}_l(r_i)$ we can write,

$${}^t\Theta(r_i, t) = \widehat{h}_l(r_i) {}^t\Theta^l(t) \quad (21)$$

where the ${}^t\Theta^l(t)$ are the interpolated values.

For the sake of simplicity, from here onwards we shall omit the indication of the independent variables for each function.

We define the mass matrix,

$$M_{ij}^J = \int_{tV} \widehat{h}_i \widehat{h}_j {}^t dv \quad (22)$$

and we want the following weak relation to be fulfilled [22],

$$\int_{tV} \widehat{h}_i \left[\widehat{h}_j {}^t\Theta^j - {}^tJ \right] {}^t dv = 0 \quad (23)$$

hence,

$${}^t\Theta^l = [(M^J)]_{li}^{-1} \int_{tV} \widehat{h}_i {}^tJ {}^t dv . \quad (24)$$

We also consistently calculate,

$$\begin{aligned} \frac{\partial {}^t\Theta}{\partial t} &= \widehat{h}_l \frac{\partial {}^t\Theta^l}{\partial t} \\ &= \widehat{h}_l [(M^J)]_{li}^{-1} \int_{tV} \widehat{h}_i \frac{\partial {}^tJ}{\partial t} {}^t dv \end{aligned} \quad (25)$$

Using the continuity equation we get,

$$\begin{aligned} \frac{\partial {}^t\Theta}{\partial t} &= \widehat{h}_j [(M^J)]_{jl}^{-1} \left[\int_{tV} \widehat{h}_l {}^tJ \frac{\partial h_k}{\partial {}^t x_i} {}^t dv \right] {}^t v_i^k \\ &\quad - \widehat{h}_j [(M^J)]_{jl}^{-1} \left[\int_{tV} \widehat{h}_l \frac{\partial {}^tJ}{\partial {}^t x_i} h_k {}^t dv \right] {}^t v_i^k \end{aligned} \quad (26)$$

We can write Eqn.(26) as,

$$\frac{\partial {}^t\Theta}{\partial t} = \Gamma_{ki}^\Theta {}^t v_i^k . \quad (27)$$

In the above equation,

$$\begin{aligned} \Gamma_{ki}^\Theta &= \widehat{h}_j [(M^J)]_{jl}^{-1} \left[\int_{tV} \widehat{h}_l {}^tJ \frac{\partial h_k}{\partial {}^t x_i} {}^t dv \right] \\ &\quad - \widehat{h}_j [(M^J)]_{jl}^{-1} \left[\int_{tV} \widehat{h}_l \frac{\partial {}^tJ}{\partial {}^t x_i} h_k {}^t dv \right] . \end{aligned} \quad (28)$$

3.2.2 Projections of ${}^t\widehat{\underline{\mathbf{F}}}$ and $\frac{\partial {}^t\widehat{\underline{\mathbf{F}}}}{\partial t}$

From Eqn.(15) we get the value of the isochoric part of the deformation gradient tensor at any point inside an element,

$${}^t\widehat{F}_{ij}(r_l, t) = (h_k(r_l) {}^tF_{ij}^k(t)) \left[\det \left(h_p(r_l) {}^t\underline{\mathbf{F}}^p(t) \right) \right]^{-\frac{1}{3}} \quad (29)$$

Let us consider ${}^t\widehat{\mathcal{F}}_{ij}(r_l, t)$ to be a projection of ${}^t\widehat{F}_{ij}(r_l, t)$. Using a new set of interpolation functions $\widehat{h}_k(r_l)$ we can write,

$${}^t\widehat{\mathcal{F}}_{ij}(r_l, t) = \widehat{h}_k(r_l) {}^t\widehat{\mathcal{F}}_{ij}^k(t) \quad (30)$$

where ${}^t\widehat{\mathcal{F}}_{ij}^k(t)$ are the interpolated values.

We define the mass matrix,

$$M_{kl}^F = \int_{tV} \widehat{h}_k \widehat{h}_l {}^t dv \quad (31)$$

and we want the following weak relation to be fulfilled,

$$\int_{tV} \widehat{h}_k \left[\widehat{h}_l {}^t\widehat{\mathcal{F}}_{ij}^l - {}^t\widehat{F}_{ij} \right] {}^t dv = 0 \quad (32)$$

hence,

$${}^t\widehat{\mathcal{F}}_{ij}^k = [(M^F)]_{kl}^{-1} \int_{tV} \widehat{h}_l {}^t\widehat{F}_{ij} {}^t dv \quad (33)$$

For the consistent time derivative we have,

$$\begin{aligned} \frac{\partial {}^t\widehat{\mathcal{F}}_{ij}}{\partial t} &= \widehat{h}_k \frac{\partial {}^t\widehat{\mathcal{F}}_{ij}^k}{\partial t} \\ &= \widehat{h}_k \left[(M^F)^{-1} \right]_{kl} \int_{tV} \widehat{h}_l \frac{\partial {}^t\widehat{F}_{ij}}{\partial t} {}^t dv \end{aligned} \quad (34)$$

and using in the above Eqn.(6b) we get,

$$\begin{aligned} \frac{\partial {}^t\widehat{\mathcal{F}}_{ij}}{\partial t} &= \widehat{h}_k \left[(M^F)^{-1} \right]_{kl} \\ &\left[\int_{tV} \widehat{h}_l {}^t\widehat{F}_{mj} \left(\frac{\partial h^p}{\partial {}^tx_m} \delta_{ri} - \frac{1}{3} \frac{\partial h^p}{\partial {}^tx_r} \delta_{im} \right) {}^t dv \right] {}^tv_r^p \\ &\quad - \widehat{h}_k \left[(M^F)^{-1} \right]_{kl} \\ &\left[\int_{tV} \widehat{h}_l \left(h^p \frac{\partial {}^t\widehat{F}_{ij}}{\partial {}^tx_r} \right) {}^t dv \right] {}^tv_r^p \end{aligned} \quad (35)$$

We can write Eqn.(35) as,

$$\frac{\partial {}^t\widehat{\mathcal{F}}_{ij}(t x_j, t)}{\partial t} = \Gamma_{ijpr}^{\widehat{\mathbf{F}}} {}^tv_r^p. \quad (36)$$

In the above equation,

$$\begin{aligned}
\Gamma_{ijpr}^{\widehat{F}} &= \widehat{h}_k \left[(M^F)^{-1} \right]_{kl} \\
\left[\int_{t_V} \widehat{h}_l \, {}^t\widehat{F}_{mj} \left(\frac{\partial h^p}{\partial {}^t x_m} \delta_{ri} - \frac{1}{3} \delta_{im} \frac{\partial h^p}{\partial {}^t x_r} \right) {}^t dv \right] \\
&\quad - \widehat{h}_k \left[(M^F)^{-1} \right]_{kl} \\
&\quad \left[\int_{t_V} \widehat{h}_l \left(h^p \frac{\partial {}^t\widehat{F}_{ij}}{\partial {}^t x_r} \right) {}^t dv \right]
\end{aligned} \tag{37}$$

3.3 Linearization of the momentum balance equations

We use a linearized approach to the momentum conservation at time $t + \Delta t$,

$$\left[{}^t R^{ext} \right]_i^k - \left[{}^t R^{int} \right]_i^k + \left[\frac{\partial \left(\left[R^{ext} \right]_i^k - \left[R^{int} \right]_i^k \right)}{\partial t} \right]_{t+\Delta t} \Delta t = 0 \tag{38}$$

in the above equation, $k = 1, \dots, NNODES$ and $i = 1, \dots, 3$.

Using Eqn. (18) and being, in our Eulerian formulation, the external loads function of time and of the spatial position we get [26],

$$\left[\frac{\partial \left[R^{ext} \right]_i^k}{\partial t} \right]_{t+\Delta t} = \int_{t_V} h_k \left[\frac{\partial (\rho \mathbf{f}_i^V)}{\partial t} \right]_{t+\Delta t} {}^t dv + \int_{t_{\partial V}} h_k \left[\frac{\partial \mathbf{t}_i}{\partial t} \right]_{t+\Delta t} {}^t dv \tag{39}$$

where the spatial volume is constant with time.

Using now Eqn. (19) we get,

$$\left[\frac{\partial \left[R^{int} \right]_i^k}{\partial t} \right]_{t+\Delta t} = \int_{t_V} \frac{\partial h_k}{\partial {}^t x_j} \left[\frac{\partial \sigma_{ij}}{\partial t} \right]_{t+\Delta t} {}^t dv. \tag{40}$$

For the finite element model we can write the hyperelastic constitutive equation (14) as,

$${}^t \sigma_{ij} = {}^t \sigma_{ij} \left({}^t \widehat{\mathcal{F}}_{lm}, {}^t \Theta \right). \tag{41}$$

Hence,

$$\frac{\partial \sigma_{ij}}{\partial t} = \frac{\partial \sigma_{ij}}{\partial \widehat{\mathcal{F}}_{lm}} \frac{\partial \widehat{\mathcal{F}}_{lm}}{\partial t} + \frac{\partial \sigma_{ij}}{\partial \Theta} \frac{\partial \Theta}{\partial t}. \tag{42}$$

Using Eqns. (27) and (36) we get,

$$\begin{aligned}
\left[\frac{\partial \sigma_{ij}}{\partial t} \right]_{t+\Delta t} &= \left[\frac{\partial \sigma_{ij}}{\partial \widehat{\mathcal{F}}_{lm}} \right]_{t+\Delta t} \left[\Gamma_{lmkr}^{\widehat{F}} \right]_{t+\Delta t} {}^{t+\Delta t} v_r^k \\
&\quad + \left[\frac{\partial \sigma_{ij}}{\partial \Theta} \right]_{t+\Delta t} \left[\Gamma_{kr}^{\Theta} \right]_{t+\Delta t} {}^{t+\Delta t} v_r^k
\end{aligned} \tag{43}$$

For the sake of simplicity we consider constant external loads; therefore, using the equations derived above we get from (38),

$$\begin{aligned}
& \int_{t_V} \left\{ \frac{\partial h_k}{\partial {}^t x_j} \left[\left(\frac{\partial \sigma_{ij}}{\partial \widehat{\mathcal{F}}_{lm}} \right)_{t+\Delta t} \left(\Gamma_{lmkr}^{\widehat{\mathcal{F}}} \right)_{t+\Delta t} \right. \right. \\
& \left. \left. + \left(\frac{\partial \sigma_{ij}}{\partial \Theta} \right)_{t+\Delta t} \left(\Gamma_{kr}^{\Theta} \right)_{t+\Delta t} \right] {}^t dv \right\} {}^{t+\Delta t} v_r^k = \\
& \frac{1}{\Delta t} \left([{}^t R^{ext}]_i^k - [{}^t R^{int}]_i^k \right).
\end{aligned} \tag{44}$$

The integral in the above expression is the consistent stiffness matrix. For the hyperelastic material considered in Eqn.(14) we can write,

$$\left[\frac{\partial \sigma_{ij}}{\partial \widehat{\mathcal{F}}_{lm}} \right]_t = \frac{G}{t\Theta} \left(\delta_{li} {}^t \widehat{\mathcal{F}}_{jm} + \delta_{lj} {}^t \widehat{\mathcal{F}}_{im} - \frac{2}{3} {}^t \widehat{\mathcal{F}}_{lm} \delta_{ij} \right) \tag{45}$$

and,

$$\left[\frac{\partial \sigma_{ij}}{\partial \Theta} \right]_t = (\delta_{ij} K - {}^t \tau_{ij}) \frac{1}{(t\Theta)^2}. \tag{46}$$

4 The numerical algorithm

Since we seek the stationary regime of the deformation processes under analysis, we develop a time stepping algorithm using Eqn. (44); the time is incremented until the stationary regime is reached:

$$\| {}^{t+\Delta t} \mathbf{y} - {}^t \mathbf{y} \| \leq VTOL \tag{47}$$

The implemented algorithm is:

1. $t = 0$
2. ${}^t \underline{\mathbf{E}} = \underline{\mathbf{1}}$
3. $ite = 0$
4. ${}^{t+\Delta t} \mathbf{y}^{(ite)} = {}^t \mathbf{y}$
5. ${}^{t+\Delta t} \underline{\mathbf{F}}^{(ite)} = {}^t \underline{\mathbf{E}}$
6. $ite = ite + 1$
7. Calculate ${}^{t+\Delta t} \Theta$ and ${}^{t+\Delta t} \widehat{\underline{\mathbf{F}}}$ with (20, 21, 24, 29, 30 and 33) using ${}^{t+\Delta t} \underline{\mathbf{F}}^{(ite-1)}$
8. Calculate ${}^{t+\Delta t} \mathbf{y}^{(ite)}$ using (44) with a direct solver
9. Calculate ${}^{t+\Delta t} \underline{\mathbf{F}}^{(ite)}$ using (9)
10. IF $\left[\begin{array}{l} \left\| {}^{t+\Delta t} \underline{\mathbf{F}}^{(ite)} - {}^{t+\Delta t} \underline{\mathbf{F}}^{(ite-1)} \right\| > FTOL \\ \text{OR. } \left\| {}^{t+\Delta t} \mathbf{y}^{(ite)} - {}^{t+\Delta t} \mathbf{y}^{(ite-1)} \right\| > VTOL \end{array} \right]$
- THEN GO TO 6
11. $t = t + \Delta t$

12. IF $\|{}^{t+\Delta t}\mathbf{v} - {}^t\mathbf{v}\| > VTOL$ THEN GO TO 3
13. The stationary regime has been reached.

It is important to notice that the intermediate steps are not in equilibrium and the momentum balance equation is only satisfied when the stationary regime is reached.

5 Numerical examples

In order to investigate the behavior of the new finite element formulation, in the present section we analyze an elastic material being drawn in a converging channel and an elastic material being expanded in a diverging channel.

For both cases we assume that the channel walls are frictionless and that the material completely fills the channel. Also two extreme cases are investigated: a very compressible material with a low Poisson coefficient, $\nu = 0.1$, and a nearly incompressible material with a high Poisson coefficient, $\nu = 0.49$. For all the examples we use as default values a Young modulus of $E = 2.1E06 \frac{kg}{cm^2}$ and $\Delta t = 1.E - 03$ sec.

The effect of different boundary conditions is also discussed.

All the cases are analyzed using 3D brick elements with 8 nodes for interpolating the velocities, ${}^t\Theta$ and ${}^t\hat{\underline{F}}$.

It is important to notice that, even though in section 3 when we presented the finite element formulation we considered a very general case with different interpolations for the different variables, in the actual numerical implementation we used the same interpolation for the three fields (${}^t\mathbf{u}$, ${}^t\Theta$ and ${}^t\hat{\underline{F}}$).

5.1 Converging channel

We consider two sets of boundary conditions:

$$\left. \begin{array}{l} \text{Case 1} \\ \text{Case 2} \end{array} \right\} \begin{array}{l} \left[\begin{array}{l} \text{Velocity prescribed at the channel outlet} \\ \text{Unloaded edge at the inlet} \end{array} \right] \text{ (pulling the material)} \\ \left[\begin{array}{l} \text{Velocity prescribed at the channel inlet} \\ \text{Unloaded edge at the outlet} \end{array} \right] \text{ (pushing the material)} \end{array}$$

In both cases $\frac{b}{H} = 0.5$ (Fig. 1).

5.1.1 Case 1

The boundary conditions for this case are:

$$\begin{aligned} {}^t v_n &= 0 \text{ on the side walls} \\ {}^t v_x &= v_{BC} = 100 \frac{cm}{sec} \text{ at the outflow boundary} \\ {}^t \underline{F} &= \underline{1} \text{ at the inflow boundary} \end{aligned}$$

where v_n is the velocity components normal to the wall.

In Fig. 1 we display the mesh (117 elements) used to solve this case.

In Figs. 2 and 3 we present the finite element results for the stationary regime for a material with $\nu = 0.1$ and in Figs. 4 and 5 the finite element results corresponding to a material with $\nu = 0.49$.

Comments:

- For both materials $\sigma_{xx} \rightarrow 0$ at the channel inlet.
- For both materials ${}^t F_{yy} \rightarrow 0.5$ at the channel outlet (theoretical result)

5.1.2 Case 2

In this case we impose:

$$\begin{aligned} {}^t v_n &= 0 \text{ on the side walls} \\ {}^t v_x &= v_{BC} = 100 \frac{\text{cm}}{\text{sec}} \text{ at the inflow boundary} \\ \sigma_{xx} &= 0 \text{ at the outflow boundary} \end{aligned}$$

Now the material is not undeformed at the inflow boundary, so we impose $\frac{\partial {}^t F_{xx}}{\partial x} = 0$ to model a constant state stress in the interval $[-\infty, 0]$. This condition is modelled by imposing,

$${}^t F_{xx}({}^t x = 0) = {}^t F_{xx}({}^t x = \Delta x) .$$

We use the same mesh shown in Fig. 1.

In Figs. 6 and 7 we present the finite element results corresponding to the stresses and deformation gradient tensor components for a material with $\nu = 0.1$. For Θ , we compare the results obtained using the original mesh and the mesh shown in Fig. 8 (207 elements). We see in Fig. 9 that even if both solutions are practically indistinguishable, when we look closer, the solutions show a converging behavior when the mesh is refined. The same observation can be made for the material with $\nu = 0.49$ (Fig. 10).

For both materials we observe a good convergence to theoretical results. As an example, we show, in Fig. 11, the values of Θ and ${}^t F_{yy}$ at the gauss points nearest the channel outlet compared with the theoretical result for the material with $\nu = 0.1$.

Also different time steps were used, in the range $10^{-5} < \Delta t < 10^{-2}$, and no significant differences were detected: convergence to theoretical results is more sensible to mesh refinement than to changes in Δt in this range.

5.2 Diverging channel

For this case $\frac{h}{H} = 2.0$ and we consider the same two sets of boundary conditions that we analyzed in the previous example.

The mesh used in the analyses of the diverging channel is shown in Fig. 12.

In Figs. 13, 14, 17 and 18 we present the results corresponding to $\nu = 0.1$ and in Figs. 15, 16, 19 and 20 the ones corresponding to $\nu = 0.49$.

5.3 Stability of the results

It is important to highlight that the pressure distributions for the cases with $\nu = 0.49$ do not present any indication of instabilities (checker modes) either in the converging or diverging channels [19] [24] [27].

6 Conclusions

A new finite element formulation was developed for modeling stationary elastic deformation processes with finite strains. The new formulation is based on an Eulerian description of motion and the deformation history is recovered by integrating the deformation gradient tensor along the streamlines.

The new formulation is stable and it provides good results for the complete range of Poisson coefficient values.

As a further step in the development of the new finite element formulation we shall incorporate the description of the free surfaces via the pseudo-concentrations technique [6] [7].

Acknowledgement 1 *We thankfully acknowledge the support from the TENARIS Group and from SIDERAR (Argentina)*

References

- [1] E.N.Dvorkin, M.A.Cavaliere and M.B.Goldschmit, “Finite element models in the steel industry. Part I: simulation of flat product manufacturing processes”, *Computers & Structures*, **81**, pp.559-573, 2003.
- [2] O.C.Zienkiewicz, P.C.Jain and E.Oñate, “Flow of solids during forming and extrusion: some aspects of numerical solutions”, *Int.J.Solid Struct.*, **14**, pp.15-28, 1977.
- [3] P.Perzyna, “Fundamental problems in viscoplasticity”, *Advances in Applied Mechanics*, **9**, Academic Press, 1966.
- [4] E.N.Dvorkin and E.G.Petöcz, “An effective technique for modelling 2D metal forming processes using an Eulerian formulation”, *Engng. Computations*, **10**, pp.323-336, 1993.
- [5] E.N.Dvorkin, M.A.Cavaliere and M.B.Goldschmit, “A three field element via augmented Lagrangian for modelling bulk metal forming processes”, *Computational Mechanics*, **17**, pp.2-9, 1995.
- [6] E.Thompson, “Use of the pseudo-concentrations to follow creeping viscous flows during transient analysis”, *Int.J.Num.Meth.Fluids*, **6**, pp.749-761, 1986.
- [7] E.Thompson and R.E.Smelser, “Transient analysis of forging operations by the pseudo-concentrations method”, *Int.J.Num.Meth.Engng.*, **25**, pp.177-189, 1988.
- [8] E.N.Dvorkin, M.B.Goldschmit, M.A.Cavaliere, P.M.Amenta, O.Marini and W.Stroppiana, “2D finite element parametric studies of the flat rolling process”, *J.Materials Processing Technology*, **68**, pp.99-107, 1997.
- [9] E.N.Dvorkin, M.A.Cavaliere, M.B.Goldschmit and P.M.Amenta, “On the modeling of steel product rolling processes”, *Int.J.Forming Processes (ESAFORM)*, **1**, pp.211-242, 1998.
- [10] M.A.Cavaliere, M.B.Goldschmit and E.N.Dvorkin, “Finite element analysis of steel rolling processes”, *Computers & Structures*, **79**, pp.2075-2089, 2001.
- [11] M.A.Cavaliere, M.B.Goldschmit and E.N.Dvorkin, “Finite element simulation of the steel plates hot rolling process”, *Int. J. Numerical Methods in Engng.*, **52**, pp.1411-1430, 2001.
- [12] E.N.Dvorkin and R.G.Toscano, “A new rigid-viscoplastic model for simulating thermal strain effects in metal forming proceses”, *Int. J. Numerical Methods in Engng.*, (in press)
- [13] O.C.Zienkiewicz, “Flow formulation for numerical solution of forming processes” in *Numerical Analysis of Forming Processes* (Ed. J.F.T. Pittman et al), John Wiley & Sons, 1984.
- [14] R.H. Wagoner and J.-L. Chenot, *Metal Forming Analysis*, Cambridge University Press, 2001.
- [15] B. Plohr and D.Sharp, “A conservative Eulerian formulation of the equations of elastic flow”, *Adv. Appl. Math.*, **9**, pp. 481-499, 1989.
- [16] L.E.Malvern, *Introduction to the Mechanics of a Continuous Medium*, Prentice-Hall, Englewood Cliffs, NJ, 1969.
- [17] J.E.Marsden and T.J.R.Hughes, *Mathematical Foundations of Elasticity*, Dover Publications, 1983.

- [18] J.C. Simo, T.J.R. Hughes, *Computational Inelasticity*, Springer-Verlag, 1998.
- [19] O.C.Zienkiewicz and R.L.Taylor, *The Finite Element Method*, McGraw-Hill, 1989.
- [20] Brooks A.N., and T.J.R. Hughes, "Streamline upwind Petrov-Galerkin formulations for convection dominated flows with particular emphasis on the incompressible Navier-Stokes equation", *Comp. Meth. Appl. Mech. Engrg.*, **32**, pp. 199-259, 1982.
- [21] T.J.R Hughes y A.N. Brooks, "A theoretical framework for Petrov-Galerkin methods with discontinuous weighting functions: Application to the streamline-upwind procedure", *Finite Element Fluids*, Chapter 3, pp. 47-65, John Wiley & Sons, 1982.
- [22] J.C. Simo, R.L. Taylor and K.S. Pister, "Variational and projection methods for the volume constraint in finite deformation elasto-plasticity", *Comp. Meth. Appl. Mech. Engrg.*, **51**, pp. 177-208, 1985.
- [23] R.W. Ogden, *Non-linear Elastic Deformations*, Dover Publications, 1997.
- [24] K.J.Bathe, *Finite Element Procedures*, Prentice Hall, 1996.
- [25] A. Agrawal and P.R. Dawson, "A comparison of Galerkin and streamline techniques for integrating strains from an Eulerian flow field", *Int. J. Numerical Methods in Engng.*, **21**, pp. 853-881, 1985.
- [26] T. Belytschko, W.K. Liu and B. Moran, *Nonlinear Finite Elements for Continua and Structures*, John Wiley and Sons, 2000.
- [27] E.N.Dvorkin, "On the convergence of incompressible finite element formulations: the Patch Test and the Inf-Sup condition", *Engng. Computations*, **18**, pp.539-556, 2001.

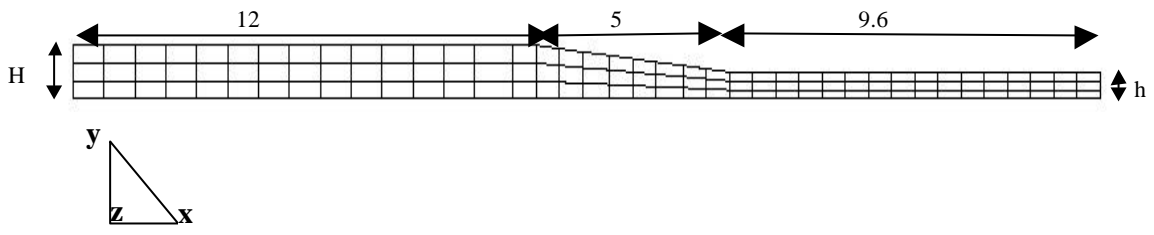


Figure 1: Converging channel. Mesh with 117 elements

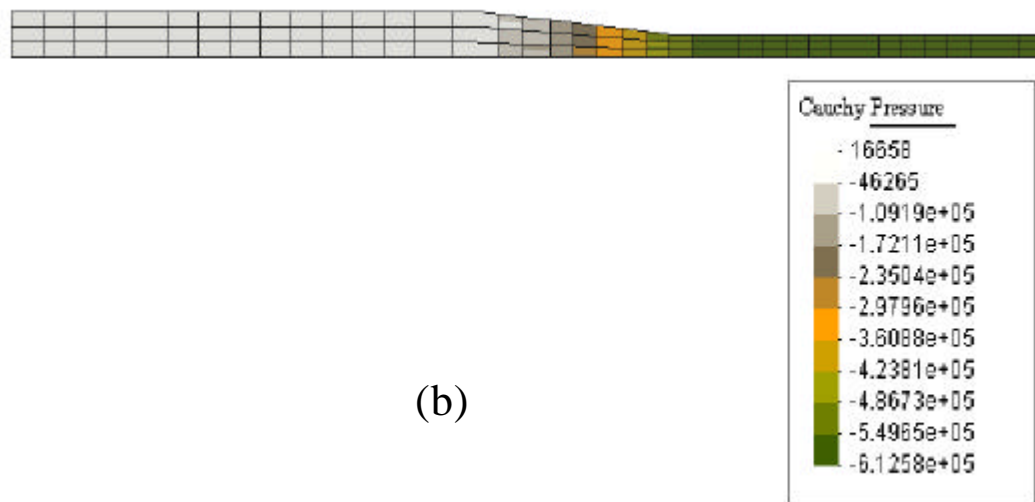
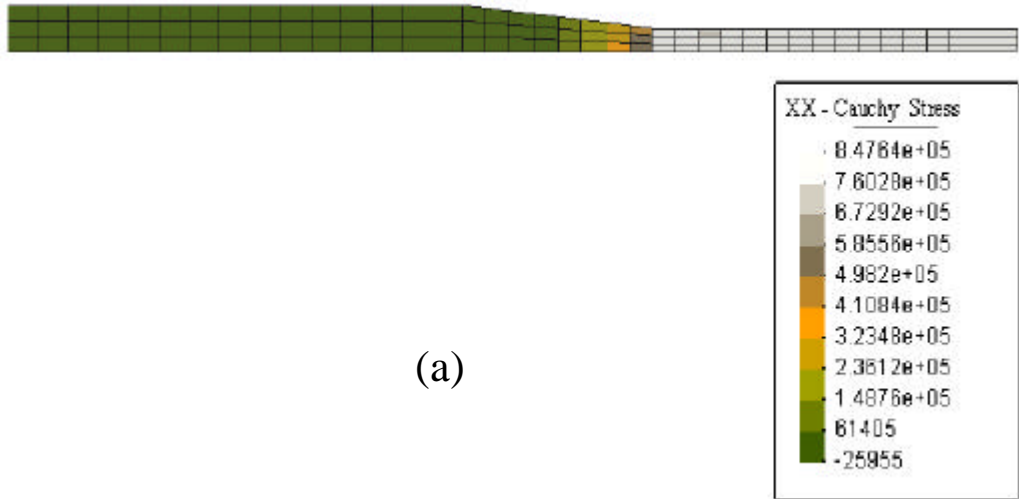
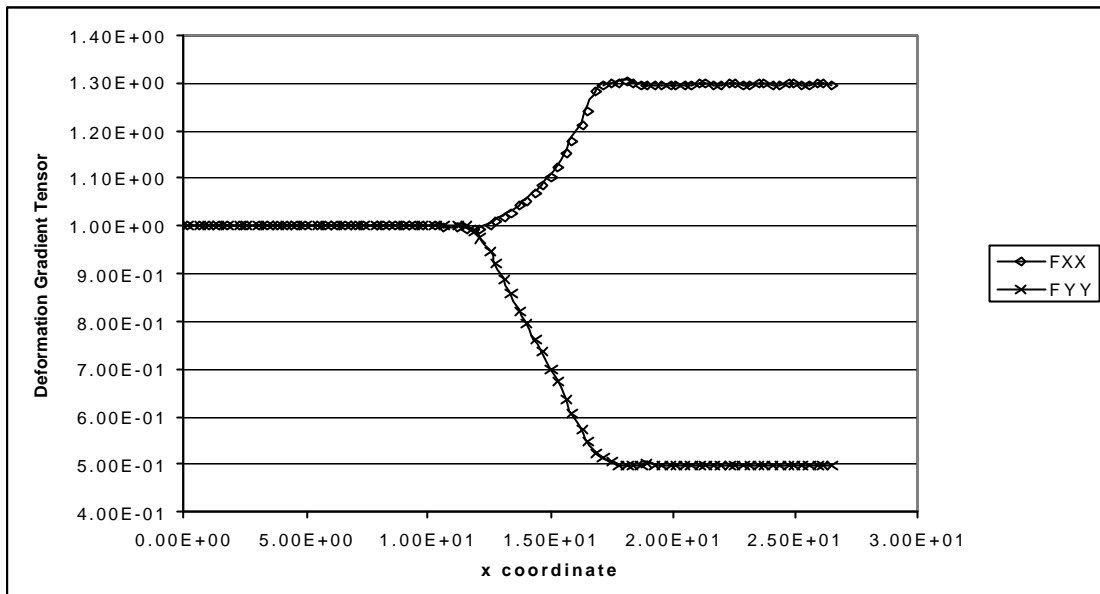
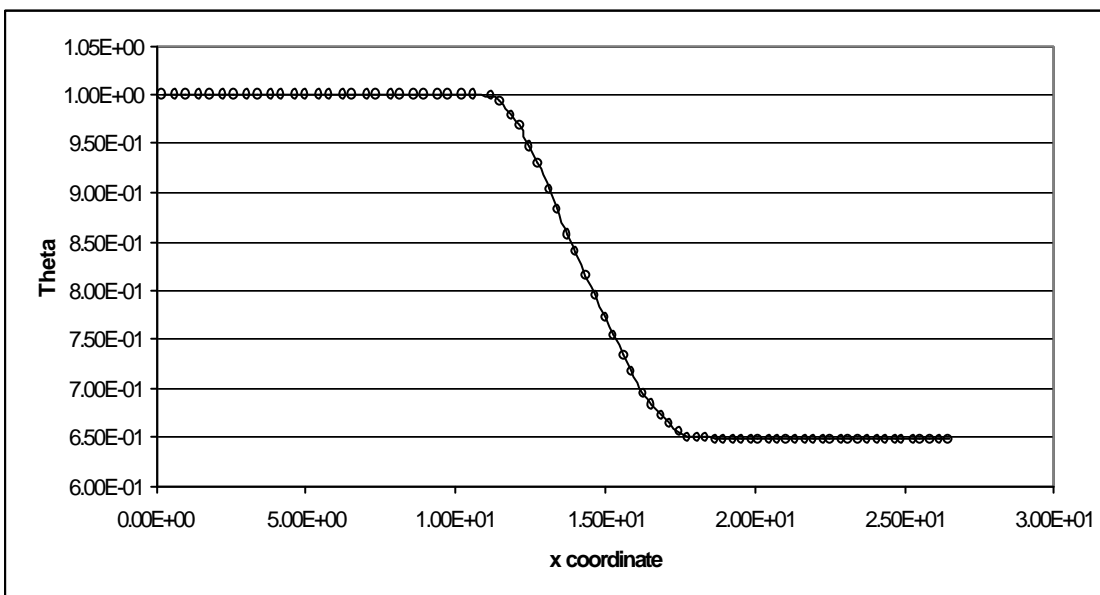


Figure 2: Converging channel. Case 1 ($\nu = 0.1$). Stresses: (a) σ_{xx} ; (b) *pressure*



(a)



(b)

Figure 3: Converging channel. Case 1 ($\nu = 0.1$). Deformation gradient tensor along the channel axis: (a) Components; (b) Θ

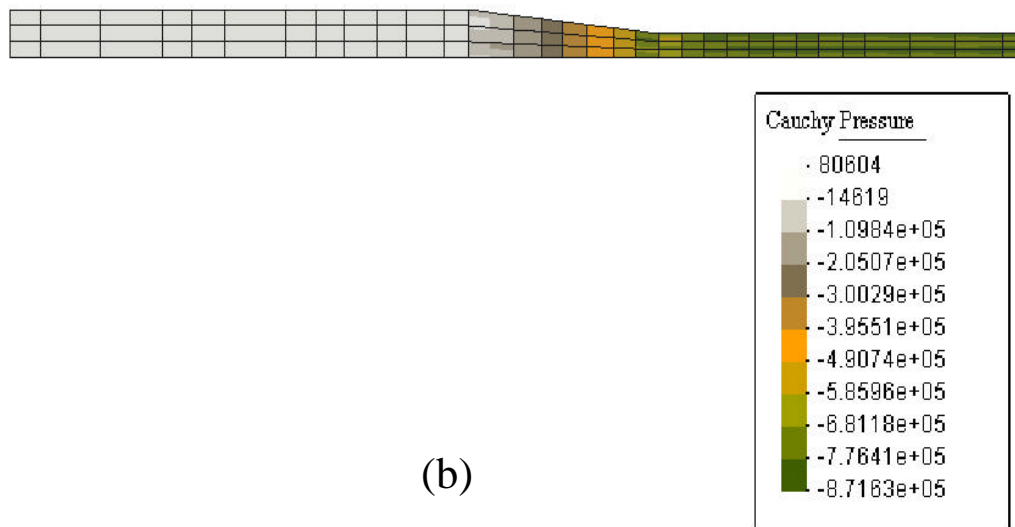
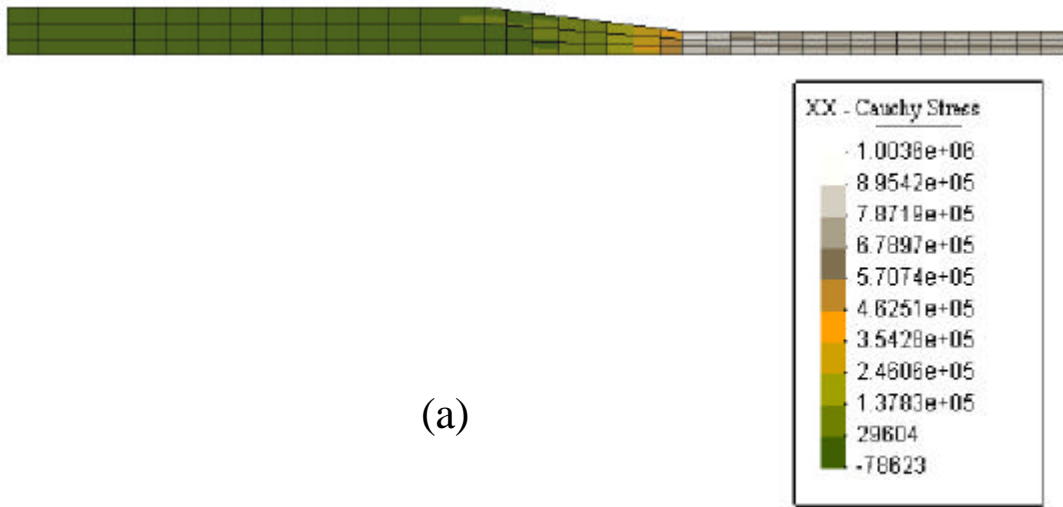
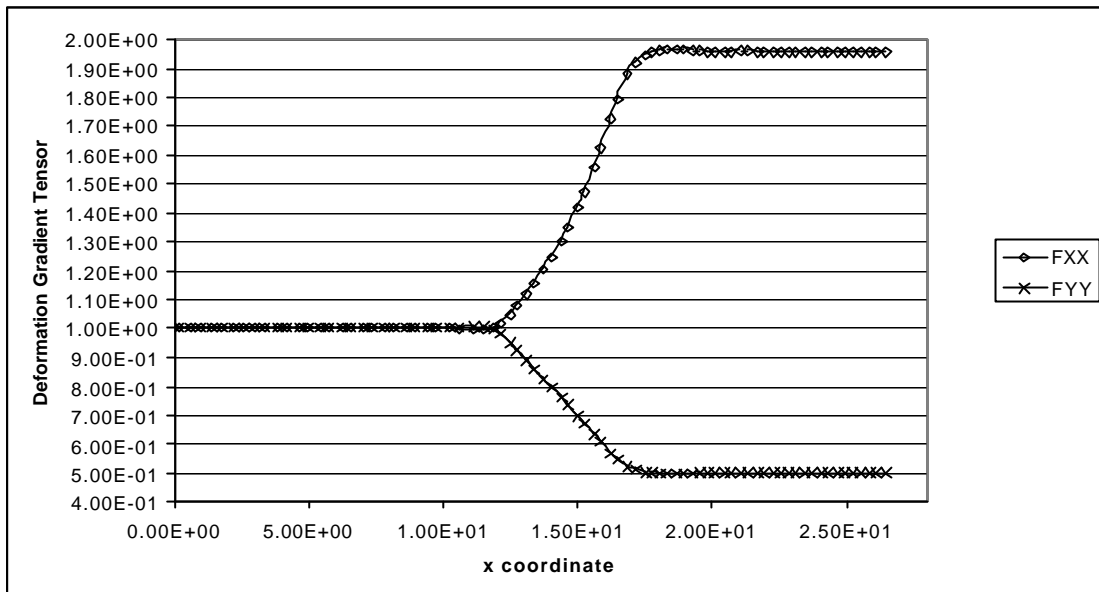
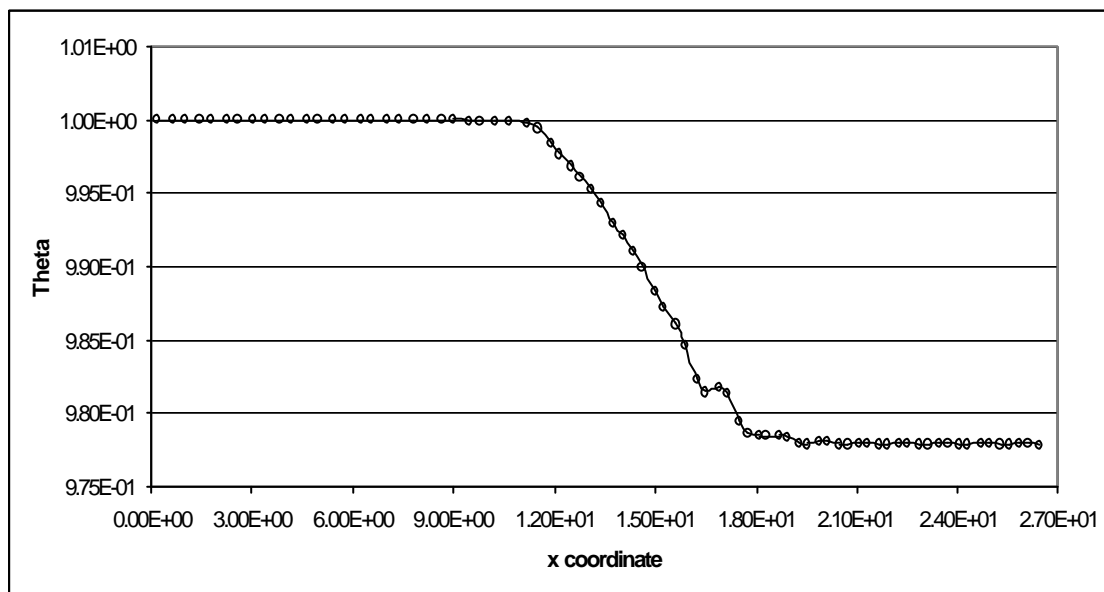


Figure 4: Converging channel. Case 1 ($\nu = 0.49$). Stresses: (a) σ_{xx} ; (b) *pressure*



(a)



(b)

Figure 5: Converging channel. Case 1 ($\nu = 0.49$). Deformation gradient tensor along the channel axis: (a) Components; (b) Θ

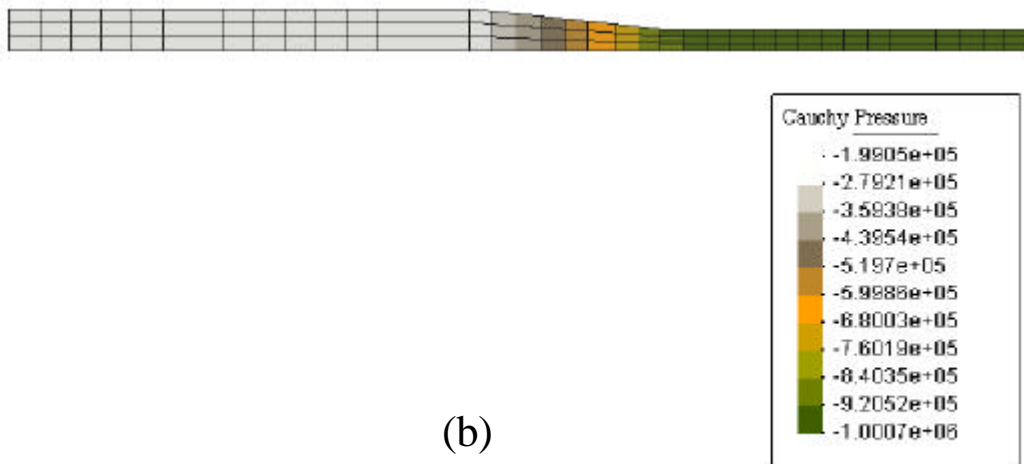
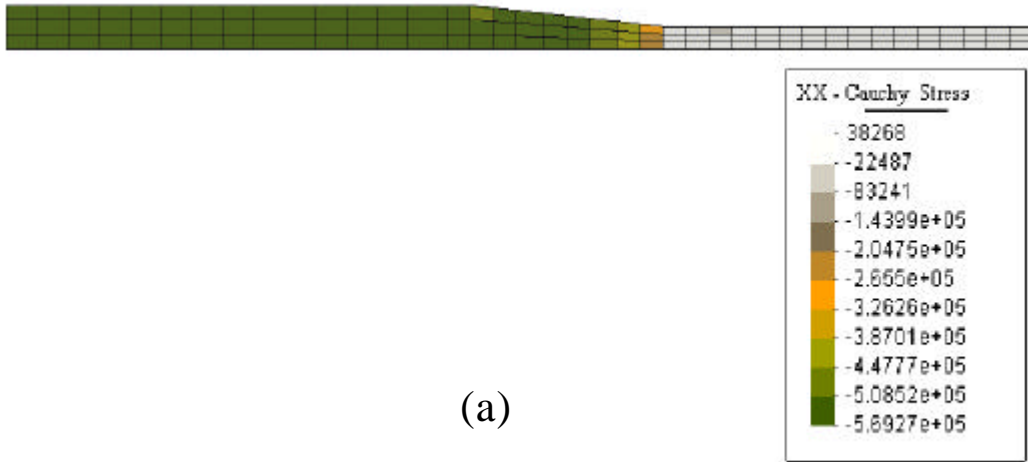


Figure 6: Converging channel. Case 2 ($\nu = 0.1$). Stresses: (a) σ_{xx} ; (b) *pressure*

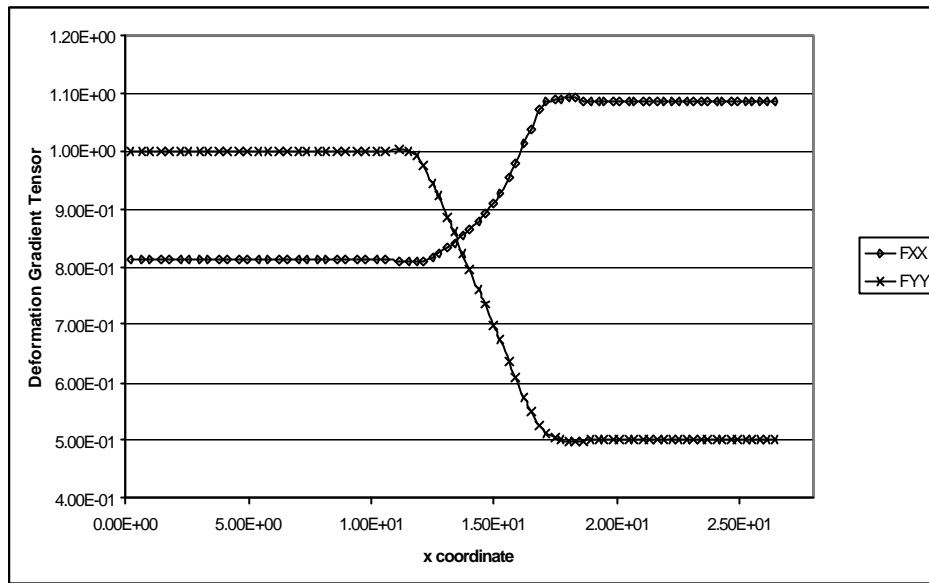


Figure 7: Converging channel. Case 2 ($\nu = 0.1$). Deformation gradient tensor along the channel axis.

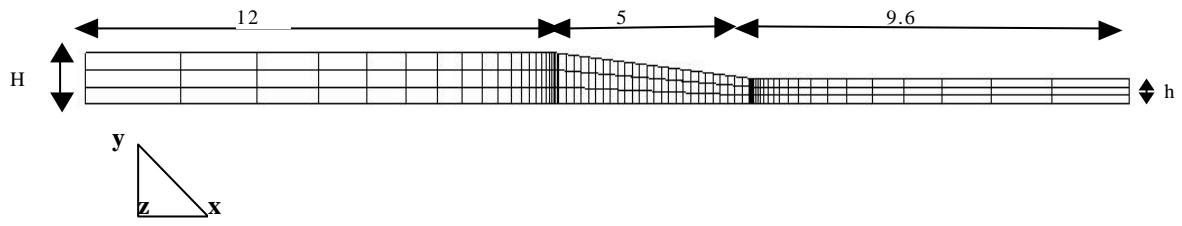


Figure 8: Converging channel. Mesh with 207 elements

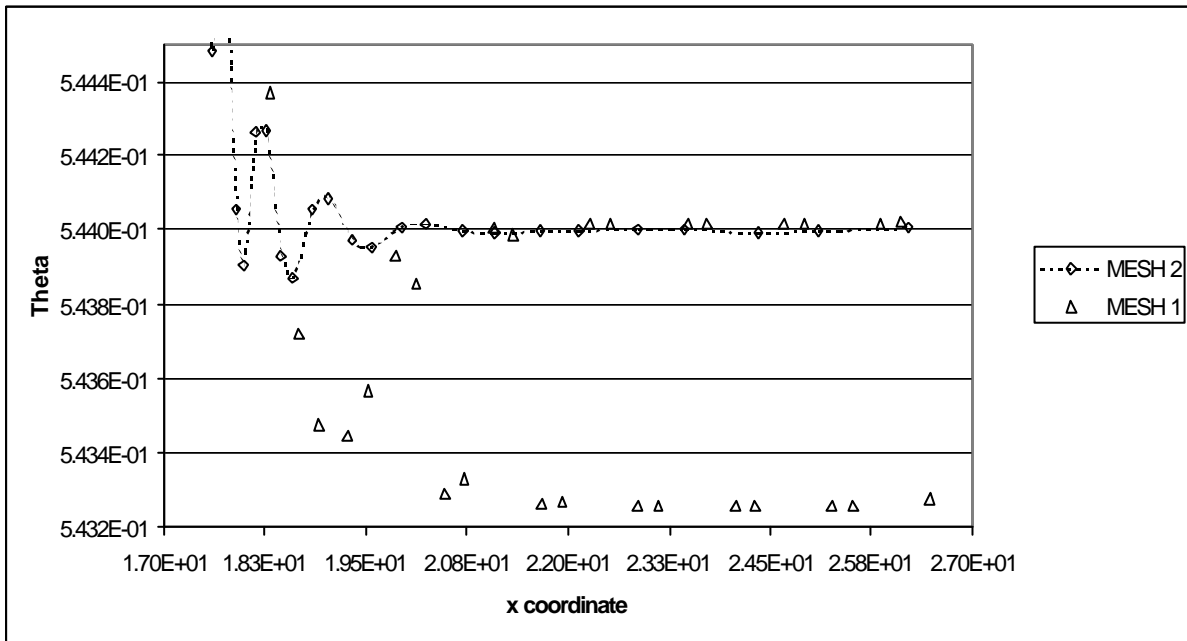
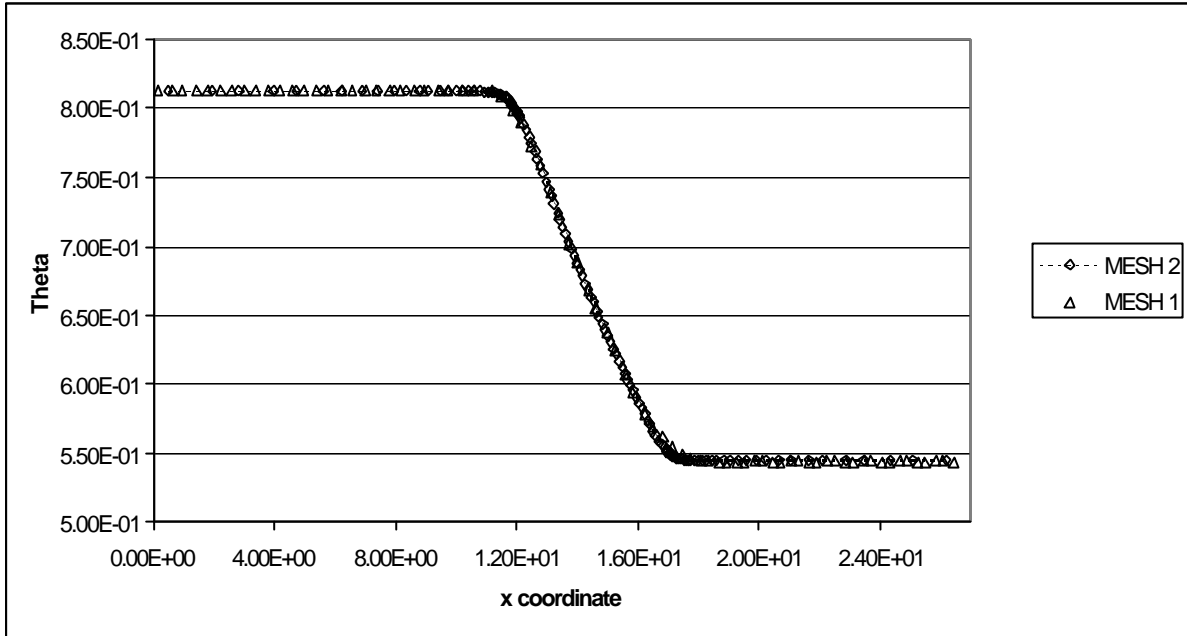


Figure 9: Converging channel. Case 2 ($\nu = 0.1$). Comparison between the meshes in Fig. 1 and in Fig. 8 (Θ)

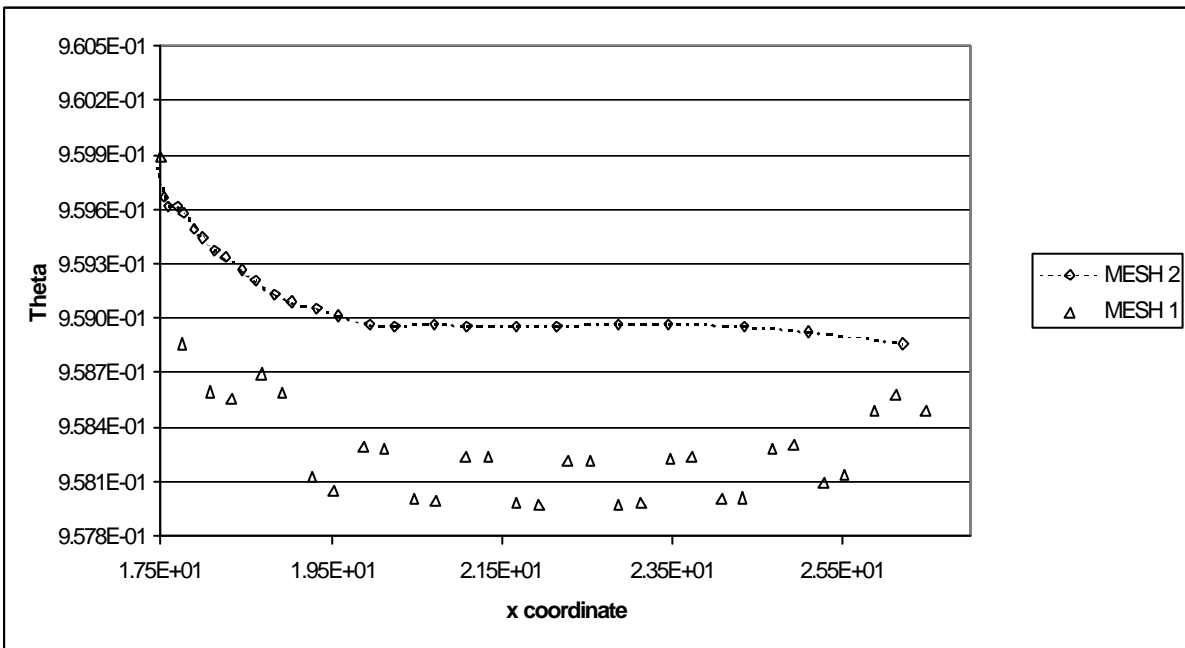
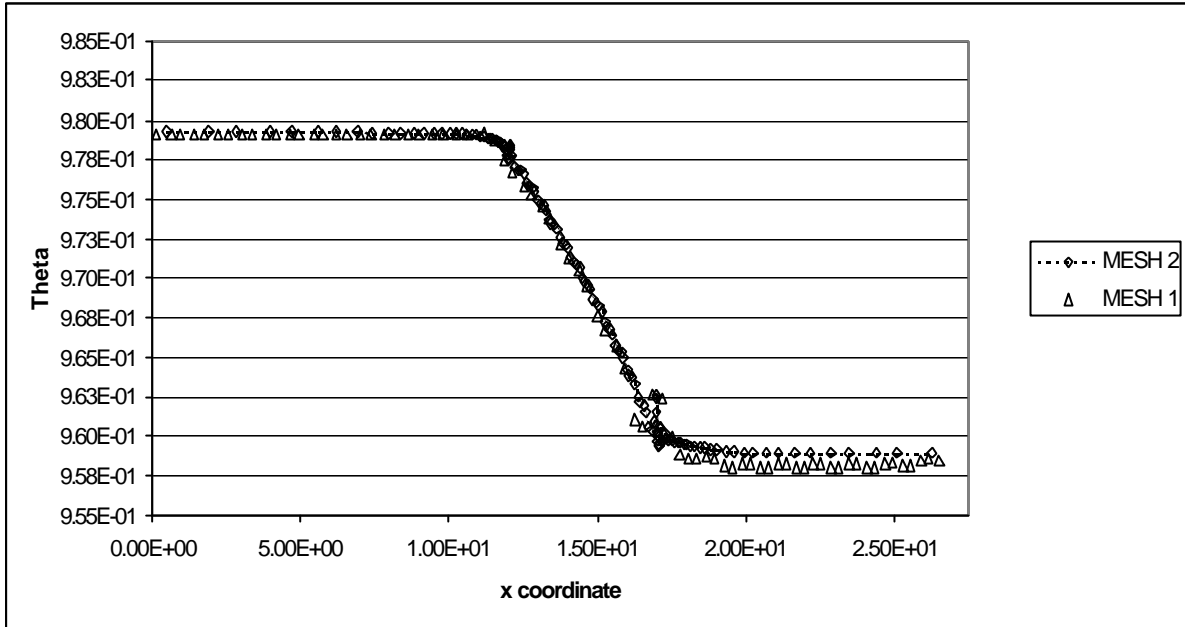


Figure 10: Converging channel. Case 2 ($\nu = 0.49$). Comparison between the meshes in Fig. 1 and in Fig. 8 (Θ)

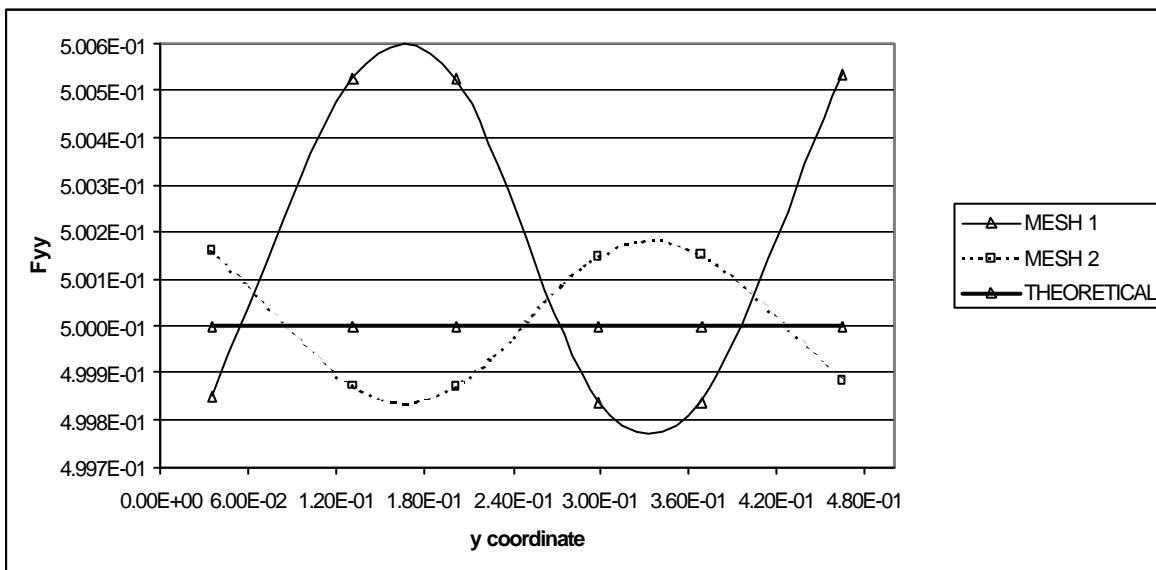
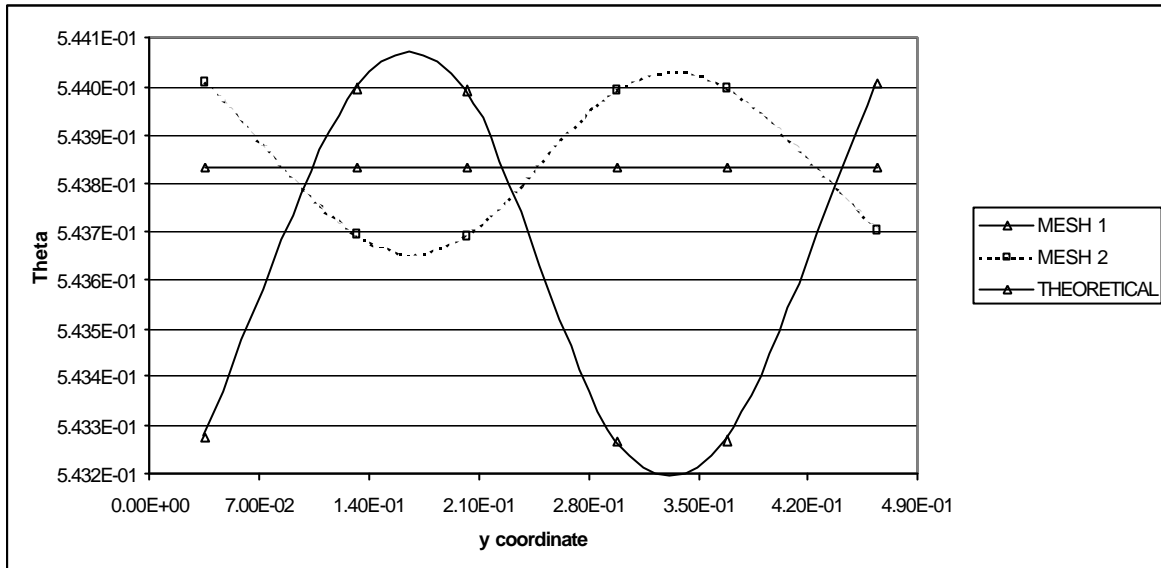


Figure 11: Converging channel. Case 2 ($\nu = 0.1$). Comparison between meshes in Fig. 1 and in Fig. 8 and theoretical values at the channel outlet

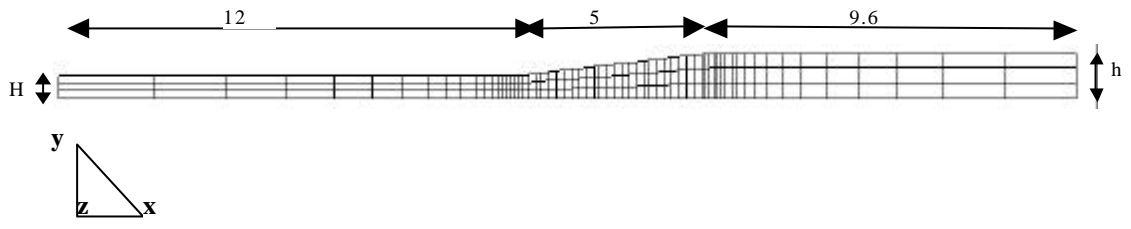


Figure 12: Diverging channel. Mesh with 207 elements

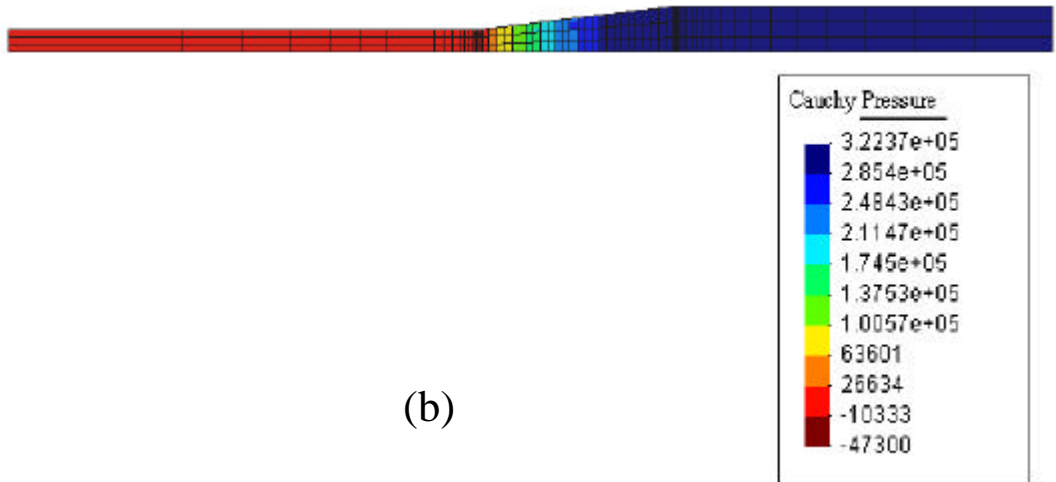
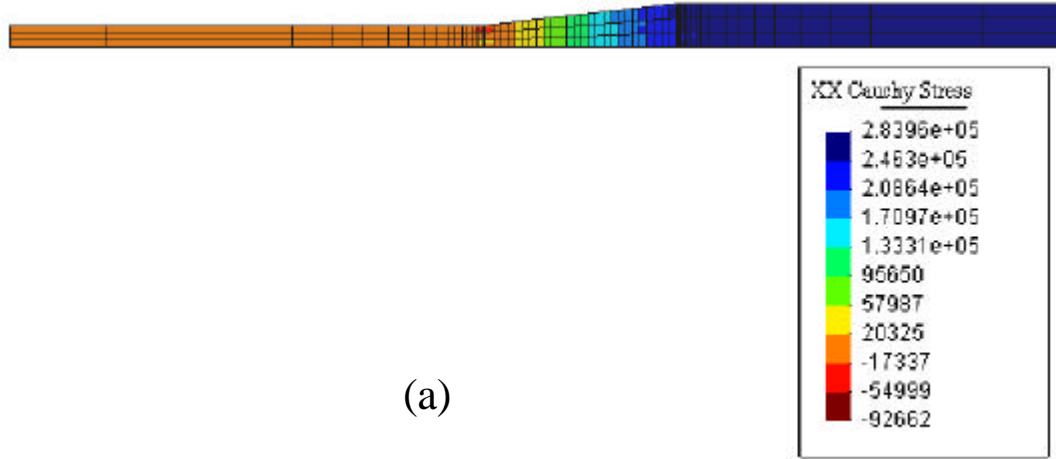
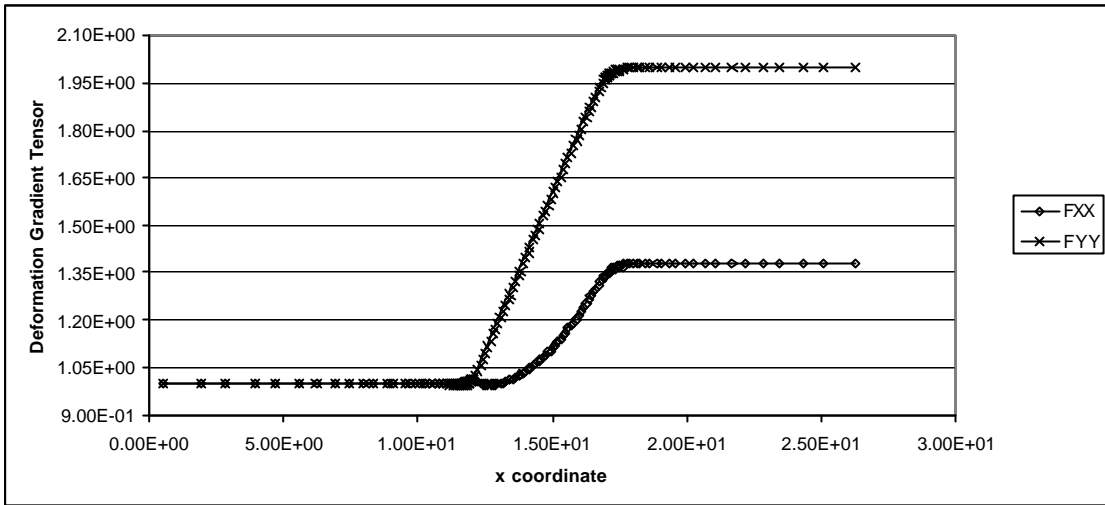
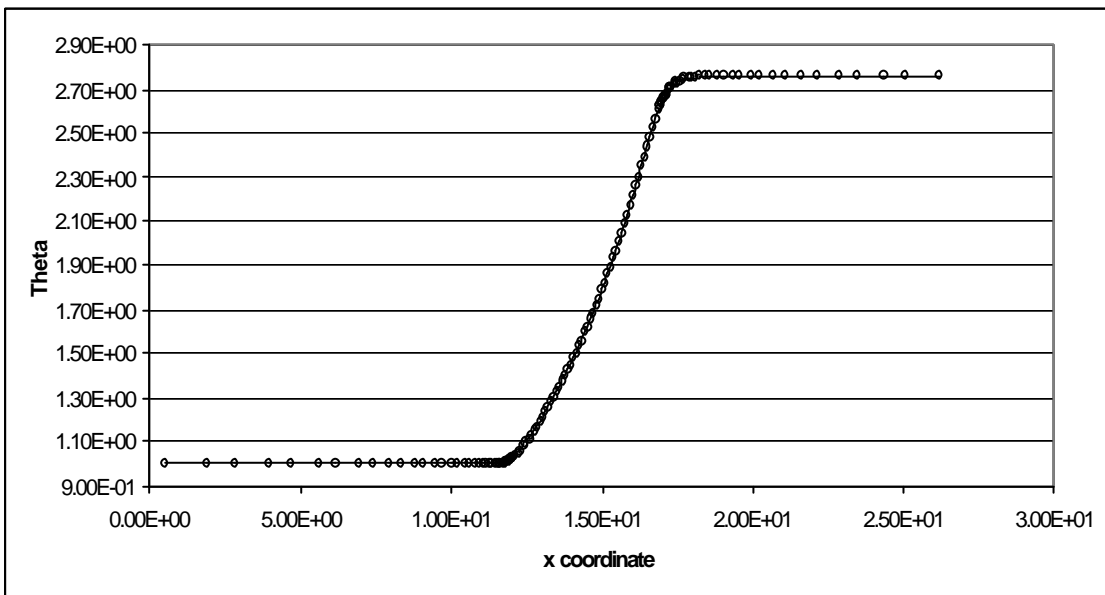


Figure 13: Diverging channel. Case 1 ($\nu = 0.1$). Stresses: (a) σ_{xx} ; (b) *pressure*



(a)



(b)

Figure 14: Diverging channel. Case 1 ($\nu = 0.1$). Deformation gradient tensor along the channel axis: (a) Components; (b) Θ

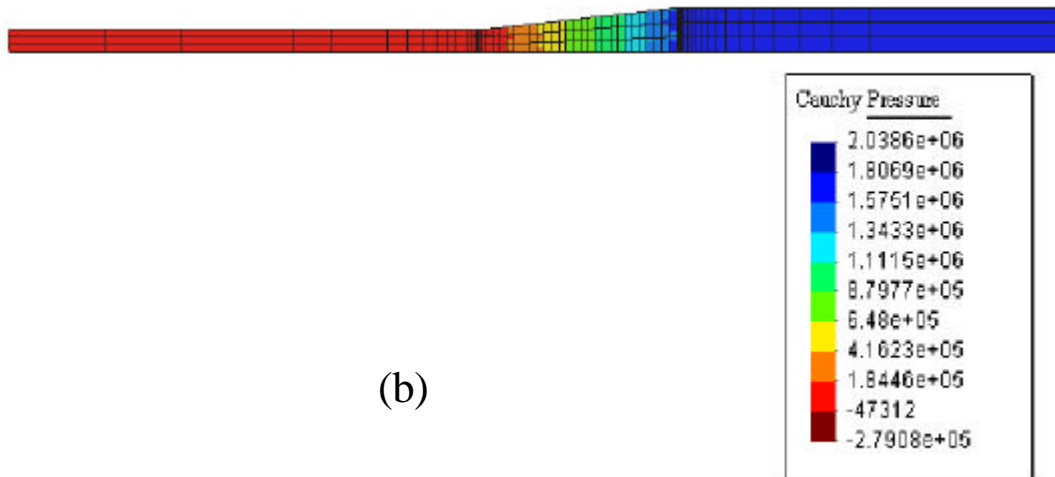
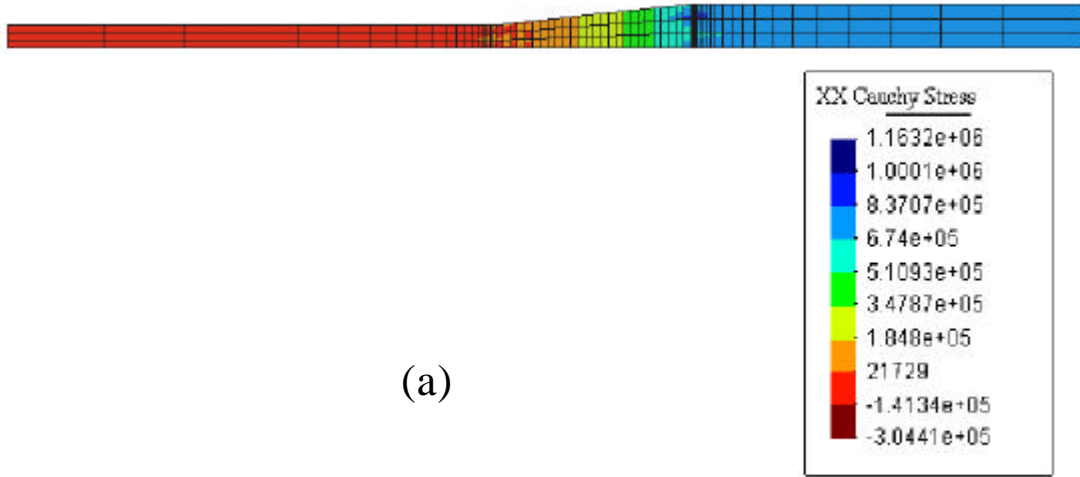
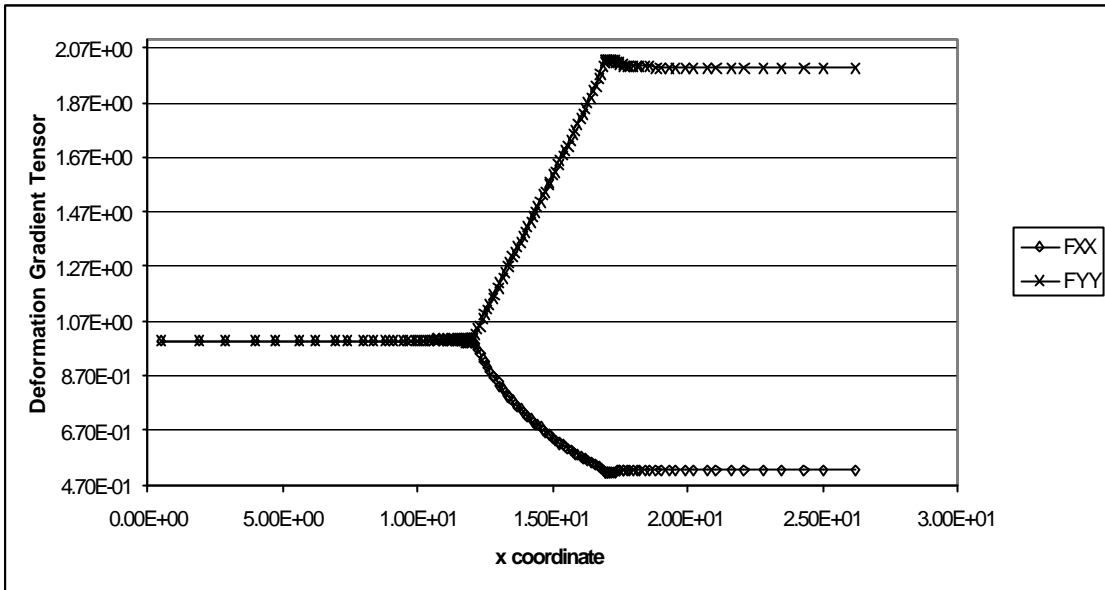
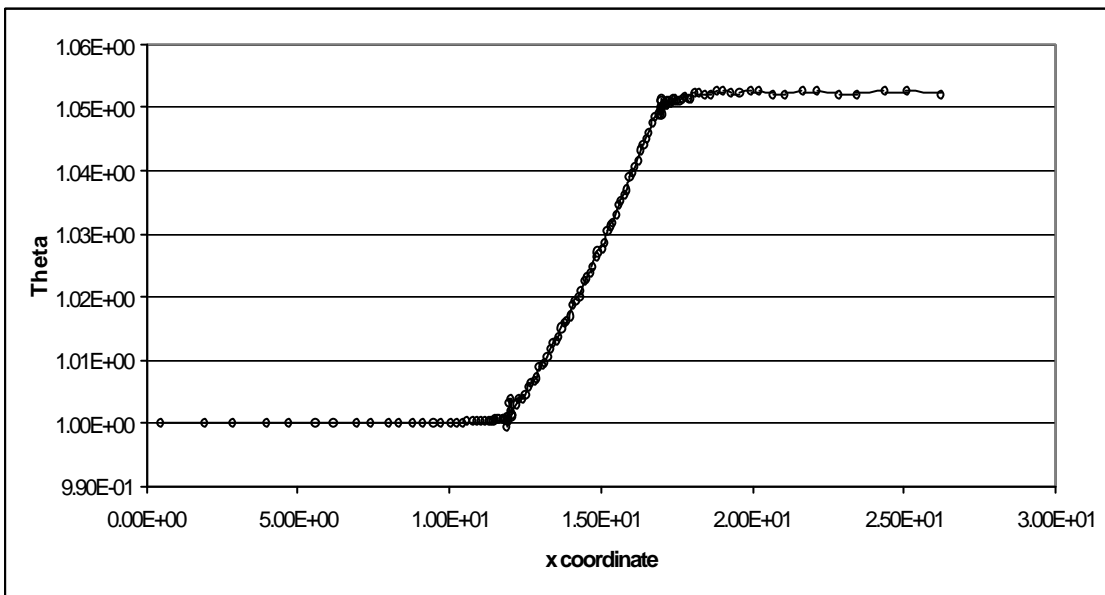


Figure 15: Diverging channel. Case 1 ($\nu = 0.49$). Stresses: (a) σ_{xx} ; (b) *pressure*



(a)



(b)

Figure 16: Diverging channel. Case 1 ($\nu = 0.49$). Deformation gradient tensor along the channel axis: (a) Components; (b) Θ

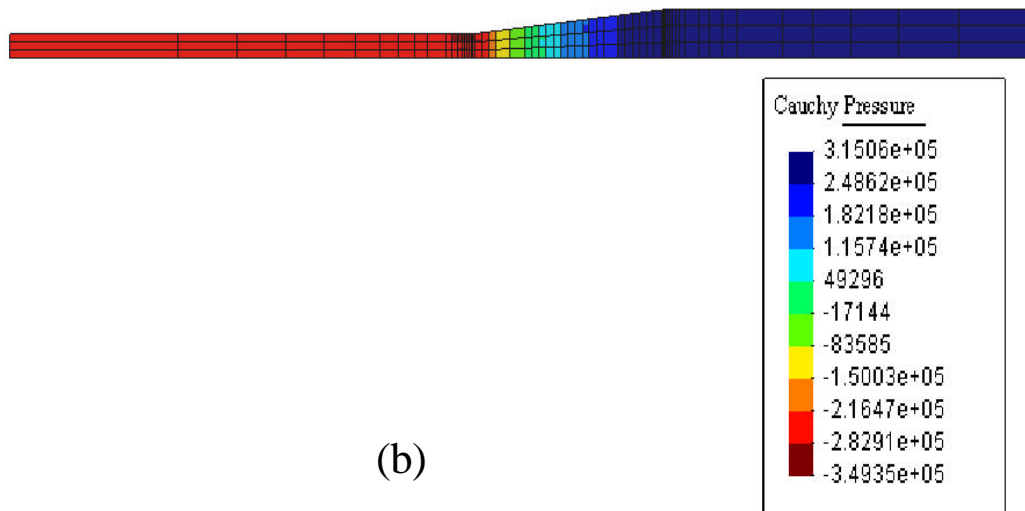
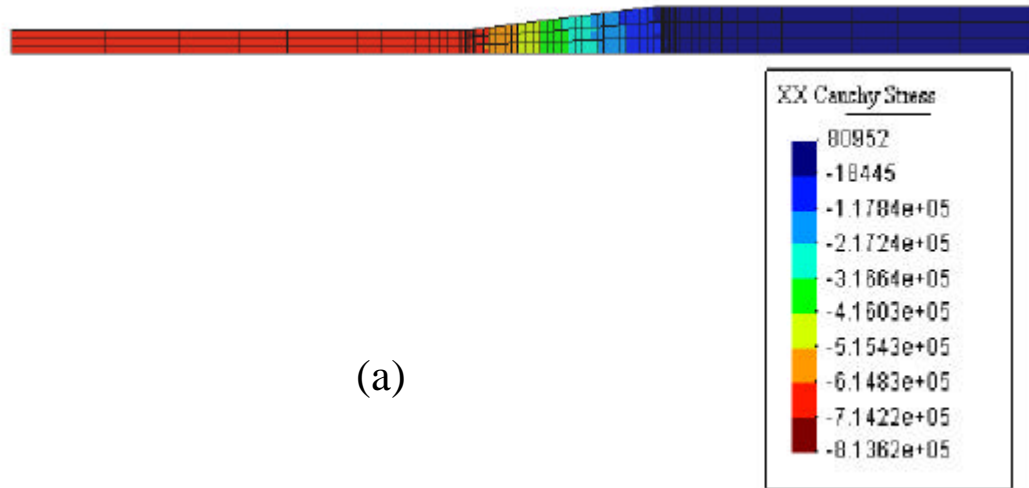
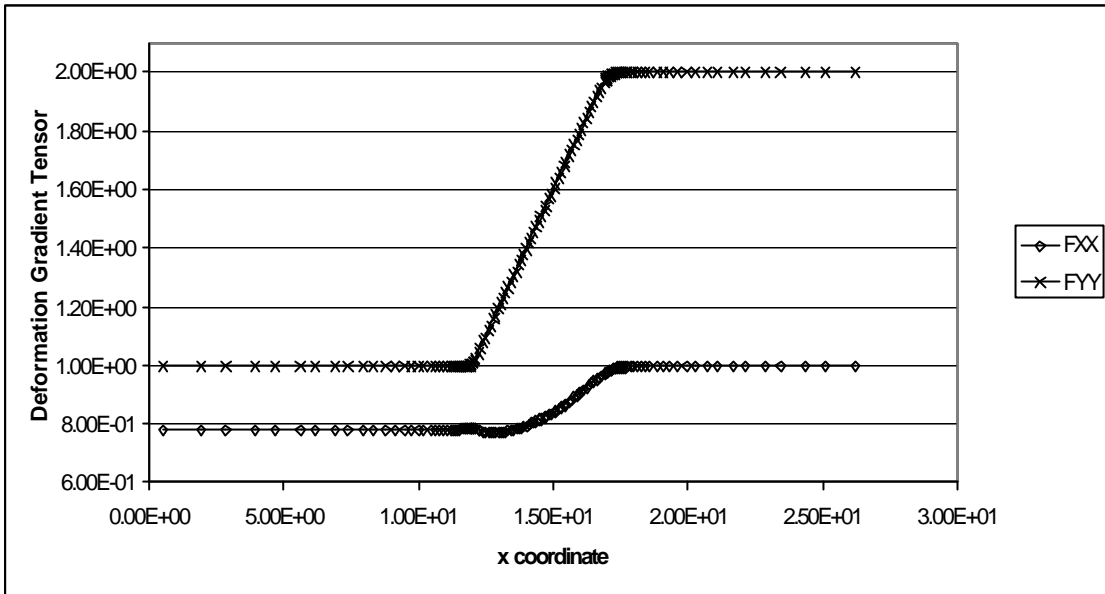
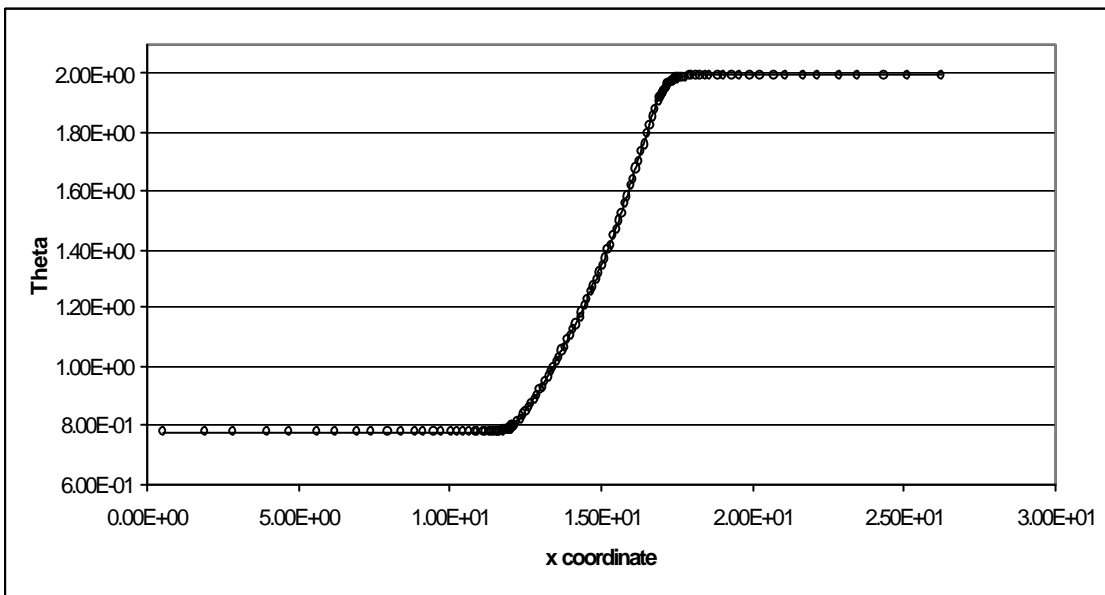


Figure 17: Diverging channel. Case 2 ($\nu = 0.1$). Stresses: (a) σ_{xx} ; (b) *pressure*



(a)



(b)

Figure 18: Diverging channel. Case 2 ($\nu = 0.1$). Deformation gradient tensor along the channel axis: (a) Components; (b) Θ

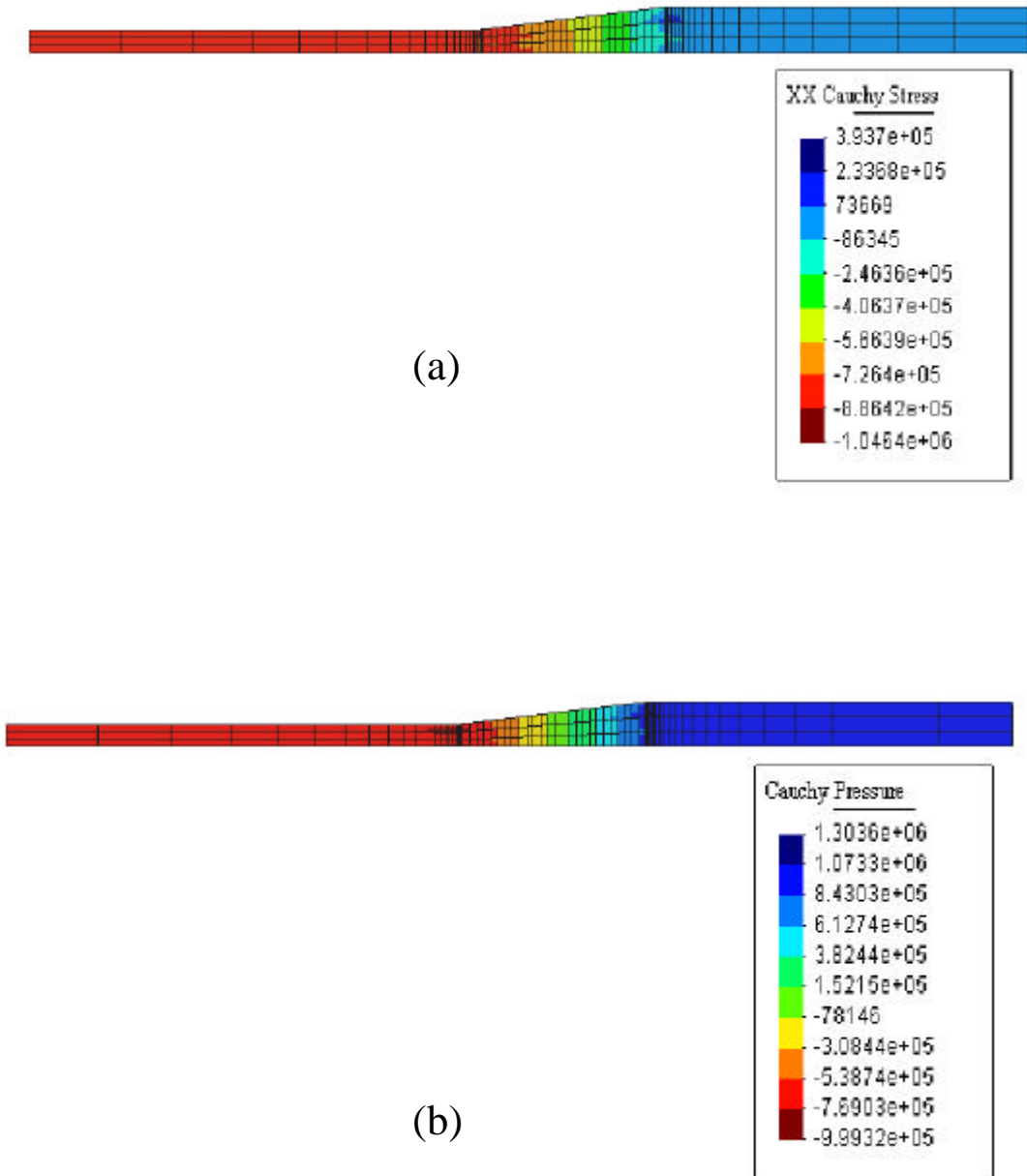
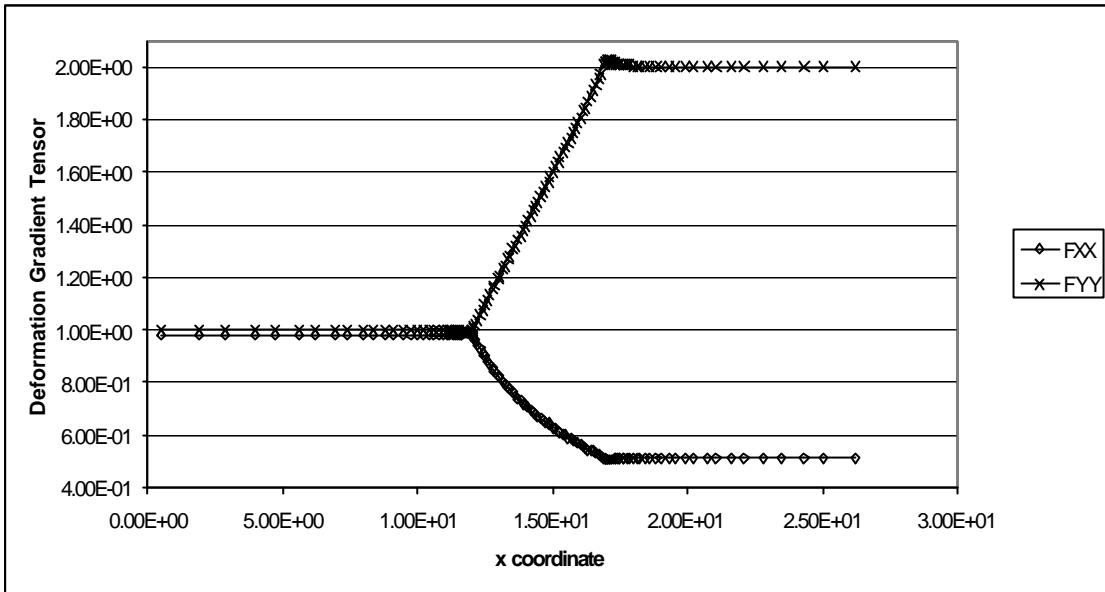
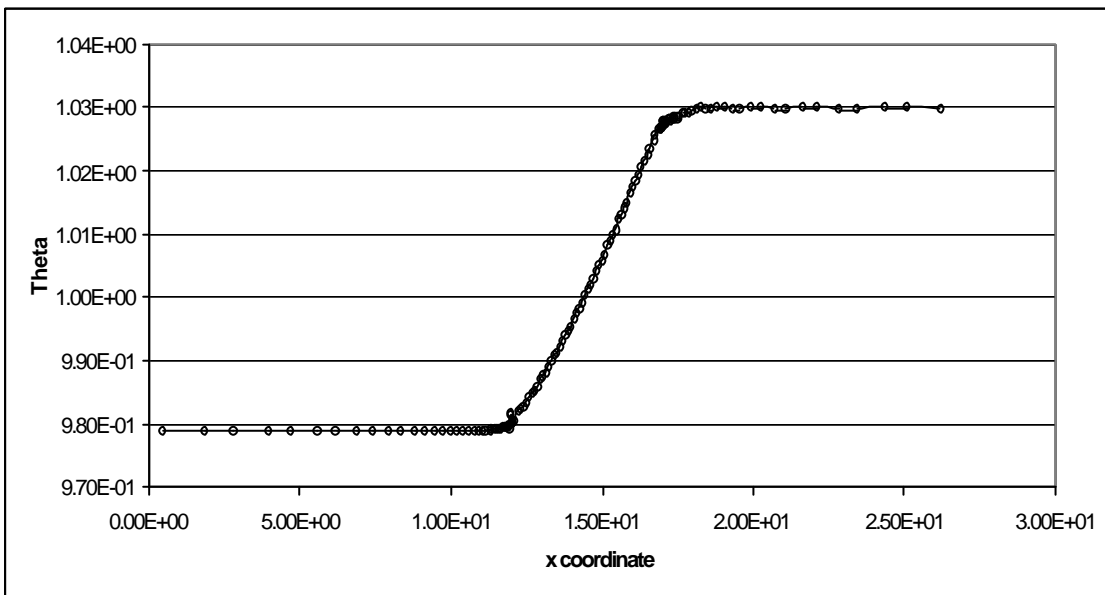


Figure 19: Diverging channel. Case 2 ($\nu = 0.49$). Stresses: (a) σ_{xx} ; (b) *pressure*



(a)



(b)

Figure 20: Diverging channel. Case 2 ($\nu = 0.49$). Deformation gradient tensor along the channel axis: (a) Components; (b) Θ